Insights into molecular plasticity in protein complexes from Trm9-Trm112 tRNA modifying enzyme crystal structure

Juliette Létoquart, Nhan van Tran, Vonny Caroline, Alexey Aleksandrov, Noureddine Lazar, Herman van Tilbeurgh, Dominique Liger, Marc Graille

Nucleic Acids Research Advance Access published October 4, 2015

Nucleic Acids Research, 2015 **1**
doi: 10.1093/nar/gkv1009

Insights into molecular plasticity in protein complexes from Trm9-Trm112 tRNA modifying enzyme crystal structure

Juliette Létoquart[1,2], Nhan van Tran[1], Vonny Caroline[1], Alexey Aleksandrov[1], Noureddine Lazar[2], Herman van Tilbeurgh[2], Dominique Liger[2,*] and Marc Graille[1,2,*]

[1]Laboratoire de Biochimie, CNRS, UMR 7654, Ecole Polytechnique, F-91128 Palaiseau Cedex, France and [2]Fonction et Architecture des Assemblages Macromoléculaires, Département B3S, Institut de Biologie Intégrative de la Cellule (I2BC), CNRS, UMR 9198, CEA, Université Paris Sud, F-91405 Orsay Cedex, France

Received March 02, 2015; Revised September 17, 2015; Accepted September 24, 2015

ABSTRACT

Most of the factors involved in translation (tRNA, rRNA and proteins) are subject to post-transcriptional and post-translational modifications, which participate in the fine-tuning and tight control of ribosome and protein synthesis processes. In eukaryotes, Trm112 acts as an obligate activating platform for at least four methyltransferases (MTase) involved in the modification of 18S rRNA (Bud23), tRNA (Trm9 and Trm11) and translation termination factor eRF1 (Mtq2). Trm112 is then at a nexus between ribosome synthesis and function. Here, we present a structure-function analysis of the Trm9-Trm112 complex, which is involved in the 5-methoxycarbonylmethyluridine (mcm^{5}U) modification of the tRNA anticodon wobble position and hence promotes translational fidelity. We also compare the known crystal structures of various Trm112-MTase complexes, highlighting the structural plasticity allowing Trm112 to interact through a very similar mode with its MTase partners, although those share less than 20% sequence identity.

INTRODUCTION

The tRNAs play a central role in protein synthesis by bringing the amino acid corresponding to the mRNA codon present in the ribosomal A-site to the ribosomal peptidyl transferase center (PTC) during the elongation step of the translation process. Post-transcriptional maturation steps are essential for tRNA function. In particular, around 100 nucleoside modifications have been described for tRNAs (1) and were shown to mostly ensure either correct tRNA folding (2) or efficient and accurate decoding (3). Position 34 from the tRNA anticodon loop (also known as wobble) is frequently heavily modified, ensuring translational fidelity but also the recognition of several codons by a single tRNA molecule. In *Saccharomyces cerevisiae*, 13 out of 42 tRNAs have a uridine at position 34 (U34), which is modified into 5-carboxymethyluridine derivatives (xcm^{5}U) in 11 of those tRNAs (4). Among these modifications, 5-methoxycarbonylmethyl-(2-thio)uridine (mcm^{5}U and mcm^{5}s^{2}U) were shown to enhance accurate and efficient translation and codon pairing (5).

The synthesis of mcm^{5}U34 is very complex and requires at least 15 proteins in *S. cerevisiae*. Most of these proteins are involved in the first step of the reaction, i.e. addition of a carboxymethyl group at position 5 of the uracil to form cm^{5}U (6). The enzyme catalyzing this reaction is the Elongator complex composed by six subunits (Elp1–6) (7). This complex consists of two sub-complexes: a core complex Elp1–2–3 where Elp3 is the catalytic subunit endowed with acetyltransferase activity and the Elp4–5–6 complex, an hexameric ATPase regulating tRNA dissociation from the Elongator complex (8). The other factors (Kti11–14, Sit4, Sap185 and Sap190) seem to be involved in the regulation of the Elongator complex (9). The last step in the synthesis of this modification requires the methylation of cm^{5}U to form mcm^{5}U by the Trm9 methyltransferase (MTase) (10). This protein belongs to the class I S-adenosyl-L-methionine (SAM)-dependent MTase family and is active as a complex with Trm112 (11). The deletion of the gene encoding any of these 15 yeast proteins results in zymocin resistance phenotype (7). Indeed, zymocin, a toxin secreted by *Kluyveromyces lactis*, exclusively cleaves the tRNA anticodon loop containing mcm^{5}s^{2}U34, thereby inhibiting translation and leading to yeast death.

Trm112 is a small zinc binding protein that in addition to Trm9 interacts with and activates 3 other MTases: Trm11, Bud23 and Mtq2. These four Trm112-MTase com-

*To whom correspondence should be addressed. Tel: +33 1 69 33 48 90; Fax: +33 1 69 33 49 09; Email: marc.graille@polytechnique.edu
Correspondence may also be addressed to Dominique Liger. Tel: +33 1 69 15 79 68; Fax: +33 1 69 85 37 15; Email: dominique.liger@i2bc.paris-saclay.fr

plexes are involved in processes related to protein synthesis. Similarly to Trm9-Trm112, the Trm11-Trm112 complex methylates many tRNAs in yeast at guanosine 10 to form 2-methylguanosine (m^2G10) and hence is involved in translational elongation (12). The Mtq2-Trm112 complex methylates translation termination factor eRF1 on the amide group of the glutamine side chain from the universally conserved GGQ motif, which enters into the PTC and triggers the release of newly synthesized proteins (13). The Bud23-Trm112 complex is implicated in the synthesis of the small ribosomal subunit by catalyzing the N^7-methylation of guanosine 1575 of 18S rRNA (14,15). Finally, Trm112 is important for synthesis of the large ribosomal subunit by an unknown mechanism (16). The Trm9-Trm112 complex catalyzed tRNA modification enhances decoding of AGA, CAA, GAA and, to a lesser extent, AGG codons (17). Hence, it favors the translation of transcripts specifically enriched in these codons such as those coding for the DNA damage response key proteins Rnr1 and Rnr3 (18). In *S. cerevisiae*, the deletion of the *TRM9* gene results in increased sensitivity of the cell to DNA alkylating agent methyl methanesulfonate (MMS) and in delayed G1 to S phase transition after MMS treatment. Furthermore, tRNA hypomodification following Trm9 inactivation results in translational infidelity and triggers the activation of protein stress response pathways (19). Altogether, this indicates a connection between tRNA modification, regulation of translation in response to stress and DNA damage response.

The Trm9-Trm112 complex is highly conserved in eukaryotes and two Trm9 orthologues exist in human: ABH8 and hTrm9L (20). Similarly to yeast Trm9-Trm112, the human ABH8-TRM112 complex converts cm^5U into mcm^5U (20). In insects, worms and human, ABH8 proteins are bifunctional enzymes also encompassing an AlkB-like domain responsible for the hydroxylation of mcm^5U into (S)-5-methoxycarbonylhydroxymethyluridine ((S)-$mchm^5U$)(21). Compared to ABH8, hTrm9L is made of only the MTase domain (22). The ABH8 protein is highly expressed in a variety of human cancer cells. Furthermore, ABH8 silencing induces apoptosis of urothelial carcinoma cells thereby suppressing tumor growth, angiogenesis and metastasis (23). On the opposite, hTrm9L has been described as a negative regulator of tumor growth (24). Interestingly, ABH8 silencing renders cells sensitive to MMS and to the anti-cancer drug bleomycin, while the loss of the gene encoding hTrm9L renders tumor cells sensitive to paromomycin and gentamycin, two antibiotics known to induce translational errors (24). Hence, human hTrm9L and ABH8 proteins represent potent targets for the development of new anti-cancer drugs.

Here, we describe the crystal structure of the Trm9-Trm112 complex from *Yarrowia lipolytica* as well as *in vivo* and *in vitro* functional studies of *S. cerevisiae* enzyme with the aim of analyzing the mechanism of action of this protein. From the comparison of the various known crystal structures of Trm112-MTase complexes, we also unravel the molecular plasticity allowing Trm112 to interact with its various MTase partners, which share less than 20% sequence identity.

MATERIALS AND METHODS

Yeast strains, media and growth conditions

Saccharomyces cerevisiae strain YPH499 (Agilent technologies) was used as the wild-type host for all yeast gene manipulations. *Kluyveromyces lactis* AWJ137 and NK40 strains were used as source of zymocin and control strain, respectively, in zymocin killer eclipse assay and killer liquid assay (25).

Cultures were performed at 30°C in standard rich medium YEPD (1% yeast extract, 2% peptone, 2% dextrose) or selective minimal media (SD) with 2% dextrose or galactose. Yeast was transformed by the lithium acetate method as previously described (26). For selection, YEPD was supplemented with geneticin (200 μg/ml) and SD minus uracil or tryptophan was prepared.

Yeast strains construction

For clone selection, three steps were systematically considered: growth on a selective media, polymerase chain reaction (PCR) screening and DNA sequencing. For point mutation strain selection, the presence of the mutation was also investigated by restriction fragment length polymorphism prior to DNA sequencing.

Trm9 point mutant strains were generated using genomic DNA from strain YDL201 (YPH499 *TRM9::kanMX6*) as DNA template and the suitable Ftrm9/R1-trm9 set of primers for initial cassette amplification (27) and the technique already described (28) (Supplementary Tables S2 and S3).

Clones expressing wild-type or mutant Trm9–13Myc were obtained from transformation of the appropriate strain (encoding wild-type or mutant Trm9) with PCR product amplified from pFA6a-13Myc-TRP1 plasmid as a template using F2-Trm9/R1-trm9 primer set (27).

The *trm9Δ::URA3* strain was obtained by transforming wild-type strain with PCR product amplified from plasmid pESC-URA (Agilent Technologies) using F1-URA-trm9/R1-URA-trm9 primer set. Clones expressing *Yl*Trm9 or *Yl*Trm9N38 were obtained from a 5-FOA selection after transformation of *trm9Δ::URA3* strain with PCR product amplified from *Yarrowia lipolytica* genomic DNA as a template using respectively Ftrm9::YLTRM9 or Ftrm9::YLTRM9N38 / Rtrm9::YlTRM9 primer sets (Supplementary Table S3).

Zymocin killer eclipse assay

5 μl suspension of the yeast cells to test (OD_{600nm} = 0.5) were spotted on YEPD plate and air-dried. Next, using the tip of a toothpick, *K. lactis* AWJ137 and NK40 cells were placed onto the edge of the yeast spot. Plate was incubated at 30°C for 1–2 days. Sensitivity or resistance to zymocin was revealed by the presence or absence of a halo zone around AWJ137 colony.

Zymocin liquid killer assay

Filtered-sterile supernatants from overnight culture of *K. lactis* AWJ137 and NK40 were used as source of zymocin

and as a control, respectively. Serial dilutions of the supernatants (from 10^{-1} to 10^{-4}) were prepared in fresh selective SD media with galactose as carbon source. 5 ml sample of each dilution was inoculated at OD_{600nm} of 0.1 with yeast strain to be tested. Cultures were incubated for 20 h at 30°C. Growth was calculated as the ratio between the OD_{600nm} read for the 10^{-1} and 10^{-4} dilutions. The 100% sensitivity to zymocin was obtained from the wild-type strain.

Cloning expression and purification

A DNA sequence optimized for heterologous expression in *E. coli* was designed to encode *Yl*Trm112 (UniprotKB entry: Q6C4P5) and *Yl*Trm9 with a C-terminus His_6-tag (UniprotKB entry: Q6C999). This fragment was obtained by *de novo* gene synthesis (GenScript Corporation, Piscataway, NJ, USA) and was further subcloned into pET21-a between *Nde*I and *Xho*I sites. Two truncated forms of *Yl*Trm9 (*Yl*Trm9N19 and *Yl*Trm9N38 encompassing residues 19–324 and 38–324, respectively) were cloned in the same operon (Supplementary Tables S4 and S5). These complexes were expressed in *E. coli* BL21 (DE3) Gold (Novagen) in 800 ml autoinducing media (29) containing 10 μM $ZnCl_2$ and 100 μg/ml ampicillin, 5 h at 37°C and 15 h at 15°C.

Genes encoding wild-type *Sc*Trm9 and *Sc*Trm112 were amplified from *S. cerevisiae* S288C genomic DNA and cloned into a modified pET28a and a pACYCDUET-1 plasmids, respectively (Supplementary Tables S4 and S5). Genes encoding *Sc*Trm9 mutants were amplified from the genomic DNA isolated from YPH499 mutated strains and then cloned into pET21-a vector using *Nde*I and *Not*I restriction sites and introducing a C-terminal His_6-tag (Supplementary Tables S4 and S5). The expression of the *Sc*Trm9-Trm112 complexes was done in *E. coli* BL21(DE3)Gold strain (Novagen) co-transformed with the two vectors and cultured in 1 l of 2YT medium containing 10 μM $ZnCl_2$, 25 μg/ml chloramphenicol and 100 μg/ml ampicillin. Cultures were done at 37°C until OD_{600nm} reached 0.5–0.6, they were then shifted to 20°C and protein production was induced overnight with IPTG (final concentration of 0.5mM).

Bacteria were harvested and resuspended in 30 ml buffer A (20mM Tris-HCl pH7.5, 200mM NaCl, 5mM ß-mercaptoethanol, 10μM $ZnCl_2$) and stored at −20°C. Cells were lysed by sonication and the soluble fraction was cleared by centrifugation (15 000*g* for 30 min at 4°C). All His_6-tagged complexes were purified by Ni-NTA chromatography (QIAGEN Inc.), followed by an ion-exchange chromatography (5 ml Heparin column for *Sc* complexes and *Yl* full length complex and 5 ml MonoQ column for the *Yl* truncated forms (GE Healthcare)). The last purification step was performed on a Superdex 75 16/60 size-exclusion chromatography column (GE Healthcare) in buffer A.

Crystallization and structure solution

Crystals were grown after 3–4 days at 19°C from a mixture of *Yl*Trm9N38-Trm112 complex (10 mg/ml) with an equal volume of the crystallization solution containing 100mM tri-sodium citrate, 20% polyethylene glycol 4000 (PEG4K), 20% 2-propanol. Crystals were cryoprotected by transfer into the crystallization solution supplemented with 15 then 30% v/v ethylene glycol and then flash-frozen in liquid nitrogen. The data sets were collected at 100 K on Proxima-1 beam line (SOLEIL, St Aubin, France). The structure was solved by Zn-MAD (Multiple Anomalous Dispersion) using data sets collected at three wavelengths corresponding to inflexion, peak and remote of Zn-edge (see Table 1 for statistics). Data were processed with XDS (30) and scaled using XSCALE. The space group was I432 ($a = b = c =$ 176.2 Å) with one heterodimer per asymmetric unit, corresponding to a solvent content of 56.4%. As expected from the presence of one Trm112 protein in the asymmetric unit, one Zn atom could be located by the HYSS submodule of the PHENIX package in the 50–3 Å resolution range (31). Refinement of the Zn atom coordinates, phasing and density modification were performed with SHARP program using the 50–3 Å resolution range (32). The *Sc*Trm112 crystal structure (13) was positioned into the experimental density maps by molecular replacement using the MOLREP program (33) and then modified to match with the *Yl*Trm112 sequence. The Trm9 model was built into these maps using the COOT molecular modeling program (34). Iterative cycles of manual model rebuilding using COOT followed by refinement with PHENIX led to an almost complete model, which was then completed and refined using a higher resolution data set (2.5 Å) to yield the final model (final R and R_{free} values of 19.9% and 24.2%, respectively). The statistics for data collection and refinement are summarized in Table 1. The final model contains residues 1–124 from Trm112, residues 39–160 and 172–233 from Trm9, a zinc atom and 91 water molecules. According to PROCHECK (35), in this final model, 87% and 13% of the residues are in the most favored and in the allowed regions of the Ramachandran diagram, respectively. Due to the absence of electron density, the following regions are absent from the final model: residues 125–130 from Trm112 and 38, 161–171, 234 and the His_6 tag from Trm9.

Enzymatic assay

For enzymatic assays, total tRNAs were purified from *S. cerevisiae trm9Δ* and *elp1Δ* strains (*elp1Δ* strain is a kind gift from Dr B. Seraphin, IGBMC, France) using mostly the protocol described in Chen et al. (36). Yeast cells were grown in YEPD medium at 30°C until cell density reached 1 to 2×10^7 cells/ml. Cells were washed with water and harvested. The pellet was resuspended in one pellet volume of 0.9% NaCl then 2 volumes of phenol were added. The mixture was incubated on a rotating wheel for 30 min at room temperature. One volume of chloroform was added and the mixture was shaken for 15 min and then centrifuged for 20 min at 13000 rpm at 4°C. Aqueous phase was precipitated by 2.5 volumes of ethanol and 0.1 volume of 20% potassium acetate and washed with cold ethanol 95%. In order to remove bound amino acids, the precipitate was resuspended in 1.5 ml of 2 M Tris-HCl pH 8 (for 10 g of cells) and incubated for 90 min at 37°C. After ethanol precipitation, the pellet was resuspended in 3.4 ml of 2 M lithium acetate, 0.1 M potassium acetate pH 5 (for 10 g of cells) to remove ribosomal RNAs as described previously (37). The mix was shaken for 20 min at 4°C and centrifuged at 8000*g* for 20

Table 1. Data collection, phasing and refinement statistics

		Crystal 1		Crystal 2
Data collection				
Space group		I432		I432
Cell dimensions				
a, *b*, *c* (Å)		176.40		176.20
α, β, γ (°)		90.00		90.00
	Peak	*Inflection*	*Remote*	
Wavelength (Å)	1.2819	1.2826	1.2753	0.9801
Resolution (Å)	50–3 (3–3.17)	50–3.3 (3.3–3.5)	50–3.7 (3.7–3.97)	50–2.5 (2.5–2.65)
R_{sym} or $R_{merge\ (\%)}$	14.8 (67.7)	15.2 (63.6)	17.5(58.9)	6.9(50.1)
I / σI	20.3 (5.1)	22.1 (6.2)	10.9 (3.6)	14.2 (2.6)
Completeness (%)	99.9 (99.7)	99.9 (99.7)	99.9 (100)	97.9 (98.3)
Redundancy	20.9	23.5	6.9	4.8
Refinement				
Resolution (Å)				50–2.5
$R_{work}/R_{free\ (\%)}$				19.9/24.2
No. atoms				
Protein				1496 (Trm9) / 966 (Trm112)
Ligand/ion				1 (Zn)
Water				76
B-factors (Å2)				
Protein				49.5 (Trm9) / 64.7 (Trm112)
Ligand/ion				76.6
Water				50.9
R.m.s deviations				
Bond lengths (Å)				0.009
Bond angles (°)				1.193

min at 4°C. The pellet was extracted a second time with 1.7 ml of 2 M lithium acetate, 0.1 M potassium acetate pH 5. The pool of supernatants was dialyzed against 10 μM magnesium acetate during 2.5 h. The tRNAs were resuspended in 1 mM Tris pH 7.5, 10 mM magnesium acetate following ethanol precipitation.

The methyltransferase assay was performed in a final volume of 50 μl containing 50 mM phosphate buffer pH 7.5, 0.1 mM EDTA, 10 mM $MgCl_2$, 10 mM NH_4Cl, 0.1 mg/ml Bovine Serum Albumin, 10 μM SAM (containing 0.87 Ci/mmol of [^{3}H]-SAM, Perkin Elmer) and 1.5 pmol of Trm9-Trm112 complexes. The reaction was initiated by adding 1.5 μM of total tRNAs (75 pmol) purified from *trm9Δ* strain to the mixture. The samples were incubated at 37°C and aliquots were withdrawn at different time points. The reaction was stopped by precipitation with cold trichloroacetic acid (5%), followed by filtration on Whatman GF/C filters. The [^{3}H] incorporation was measured using a Beckman Coulter LS6500 scintillation counter. For the pH dependence enzymatic assays, phosphate buffer pH7.5 was replaced by other phosphate buffers ranging from pH 5–8. All reactions were performed in triplicates. The initial velocities (V_i) were calculated using the equation $C_{tRNA} = V_i{*}(1 - \exp(-nt))/n$ where C_{tRNA} is the concentration of methylated tRNA, t the time in minutes, V_i the initial enzyme cycling velocity and n the relaxation rate constant of V_i by fitting the experimental spots with the software ORIGIN according to Cao et al. (38).

Steady-state kinetics analyses were performed by using various tRNA (from 0.1 to 1.5 μM) or SAM (from 1 to 20 μM) concentrations. The initial rate calculated for each tRNA or SAM concentration was plotted as a function of the concentration. The data were fit to the Michaelis–Menten equation using the ORIGIN software and the K_m, k_{cat} and k_{cat}/K_m values were calculated from the curve fitting.

Equilibrium dialysis

The equilibrium dialysis set up consists of two chambers separated by a 3 kDa-cut off dialysis membrane. The experiment was performed in 100 mM Tris-HCl pH 7.5, 0.1 mM EDTA, 10 mM $MgCl_2$, 10 mM NH_4Cl. Initially, the ligand chamber contains 100 μM SAM (containing 0.87 Ci/mmol of [^{3}H]-SAM, Perkin Elmer) and the protein chamber 120 μM of Trm9-Trm112 complex. After 3 h rotation at 4°C, the SAM content of chambers is determined using a Beckman Coulter LS6500 scintillation counter.

Co-IP and western blot

The preparation of the soluble protein extracts and the co-immunoprecipitation assays were performed as previously described (26). Probing was performed using either mouse 9E10 anti-myc (Santa Cruz Biotechnology) or polyclonal rabbit anti-*Sc*Trm112 antibodies (Agrobio) as primary antibody (1/5000 dilution). Sheep anti-mouse or sheep anti-rabbit HRP-conjugated IgG were used as secondary antibody (1/5000, GE Healthcare).

Generation of *Yl*Trm9N20-Trm112 model

Residues 20–39 from *Yl*Trm9, which are missing in the crystal structure of *Yl*Trm9N38-Trm112 complex, were modeled by superimposing the crystal structure of RPA2492, the closest structural *Yl*Trm9 homologue (PDB code: 3E23), onto our structure. The SAM substrate and backbone atoms from residues 8–27 (corresponding to residues 20–39 from *Yl*Trm9) were retained from the crystal structure

3E23. Missing side chains were placed using the SCWRL4 software (39). The cm^5U residue was docked manually into the *Yl*Trm9 active site using constraints issued from the functional analysis of the various Trm9 mutants and by positioning the carboxyl group of cm^5U at a distance compatible with methyl transfer from SAM. Finally, as the loop containing R40 (corresponding to *Sc*Trm9 R39) is one residue shorter in *Yl*Trm9 than the corresponding region from RPA2492, which was used as a template to build this fragment, we applied a restraint with a force constant of 1000 kcal/mol/$Å^2$ between the carboxyl group of cm^5U and guanidinium group of R40 to position the side chain of this latter group toward the binding pocket. The atoms present in the crystal structure of *Yl*Trm9 were restrained to the experimental crystallographic position with a force constant of 5 kcal/mol/$Å^2$. The CHARMM27 force field was used (40). The complex was subsequently minimized in the CHARMM software (41) using the Powell algorithm and 10 000 steps of minimization.

2D thin layer chromatography for detection of modified nucleosides

The tRNAs obtained after *in vitro* methylation using [^{14}C]-SAM (containing 6.5 μl of [^{14}C]-SAM (58 mCi/mmol, Perkin Elmer)) were extracted with phenol/chloroform and ethanol precipitated. The tRNA pellet was dissolved in 10 μl of 50 mM ammonium acetate pH 5.3 supplemented with 1 μg of P1 nuclease from *Penicillium citrinum* (Sigma) and incubated overnight at 37°C. Digested tRNAs (2 μl) were mixed with 12μg of cold 5′ P-mononucleosides pA, pU, pG and pC and spotted on a CEL-300 cellulose plate (Merck). 5′ P-mononucleosides were separated using chromatographic solvents A, B or C as previously described (42). First dimension chromatography was performed in solvent A, and the second in either solvent B or C. The positions of the four major mononucleosides (pA, pG, pU and pC) were revealed by UV shadowing. The position of mcm^5U nucleoside carrying radiolabeled methyl group was revealed by phosphorimaging and compared with that of reference maps obtained under identical experimental conditions (43).

RESULTS AND DISCUSSION

Structure of the *Yl*Trm9-Trm112 complex

To determine the crystal structure of the Trm9-Trm112 complex, we expressed in *Escherichia coli* and purified this complex from different organisms (*Saccharomyces cerevisiae* (*Sc*), *Schizosaccharomyces pombe* (*Sp*), *Encephalitozoon cuniculi* (*Ec*) and *Yarrowia lipolytica* (*Yl*)). Unfortunately, no crystals could be obtained from these complexes formed by full-length proteins. Analyses of these purified complexes stored at 4°C for several weeks by SDS-PAGE followed by mass spectrometry peptide mass fingerprint revealed degradation of the N-terminal extremity from *Yl*Trm9. Therefore, two truncated *Yl*Trm9 forms lacking residues 1–18 or 1–37 (hereafter named *Yl*Trm9N19 and *Yl*Trm9N38, respectively) were cloned, co-expressed with *Yl*Trm112 and purified. Compared to full-length *Yl*Trm9-Trm112 complex, both truncated forms were strongly affected in their enzymatic activity of methylation toward a tRNA mixture isolated from a *S. cerevisiae trm9Δ* strain but displayed the same affinity for SAM, indicating that the N-terminal residues deleted in these constructs are required for optimal enzymatic activity (Supplementary Figure S1). Diffracting crystals were obtained for the *Yl*Trm9N38-Trm112 complex and its structure was solved by the MAD method using the anomalous signal of the zinc atom bound to Trm112. The final model was refined to 2.5 Å and yielded R and R_{free} values of 19.9% and 24.2%, respectively (Table 1, see Supplementary Figure S2 for electron density maps).

*Yl*Trm9N38 adopts the typical fold of the class I SAM-dependent MTases composed of a central seven-stranded ß-sheet surrounded by two α-helices on each side (Figure 1A). A twisted two-stranded antiparallel ß-sheet (strands ßA and ßB) is inserted between strand ß5 and helix αE and forms a lid positioned on top of the C-terminal extremity of the central ß-sheet. *Yl*Trm112 is formed by a zinc binding domain made of two α-helices (α1–2) and a four-stranded antiparallel ß-sheet as well as a helical domain of 3 α-helices (α3 to α5). The *Yl*Trm112 structure is very similar to the crystal structures of *Sc*Trm112 either in its free form (13) or bound to Bud23 (15) (rmsd of 1.21–1.38 Å; 49% sequence identity). The only major difference between *Yl*Trm112 and free *Sc*Trm112 results from a rearrangement of the C-terminal extremity from *Yl*Trm112 (corresponding to residues F122–L124). A similar rearrangement of this Trm112 region is also observed in the Mtq2-Trm112 and Bud23-Trm112 complexes and is required to avoid a steric clash between this Trm112 fragment and its MTase partner (26).

Trm9 binds mainly to Trm112 zinc-binding domain via a parallel ß-zipper interaction formed by Trm9 strand ß3 and Trm112 strand ß4, which results in the formation of an extended eleven-stranded ß-sheet (Figure 1A and B). Complex formation engages an interface area of 1160 $Å^2$ involving 20 and 21 residues from Trm112 and Trm9, respectively (Figure 1D and E). At the center of this interface, hydrophobic residues (M1, F8, V9, F43, M47, I119, P120 and F122) from Trm112 contact hydrophobic side chains from Trm9 (V59, F78, V102, A110, P112 and F116), thereby shielding this Trm9 region from exposure to solvent (Figure 1B and C). This explains the need to express Trm112 with Trm9 in *E. coli* to obtain soluble and active Trm9. This hydrophobic core is surrounded by several hydrogen bonds and salt bridges (see Supplementary Table S1 for details). Among these, the ß-zipper interaction is realized by two hydrogen bonds engaging main chain atoms from Trm9 V103 as well as P120 and F122 from Trm112 (Figure 1B). Other hydrogen bonds are formed by E100 from Trm9 with K2 and T5 from Trm112, by R115 from Trm9 with N7 and the carbonyl group of R50 from Trm112 and by A110 and E113 from Trm9 with Q10 from Trm112 (Figure 1B and C). Finally, a salt bridge is formed between Trm9 D117 and Trm112 R50. Among the Trm9 residues engaged in complex formation, E100, V102 and F116 from *Yl*Trm9 correspond to N89, L91 and F105 from *Sc*Trm9, which substitutions by Lys, Arg and Glu, respectively, were previously shown to disrupt and inactivate the *Sc*Trm9-Trm112 complex (26). It is noteworthy that the truncation of residues 263–279 from *Sc*Trm9 resulted in loss of interaction with Trm112 (11).

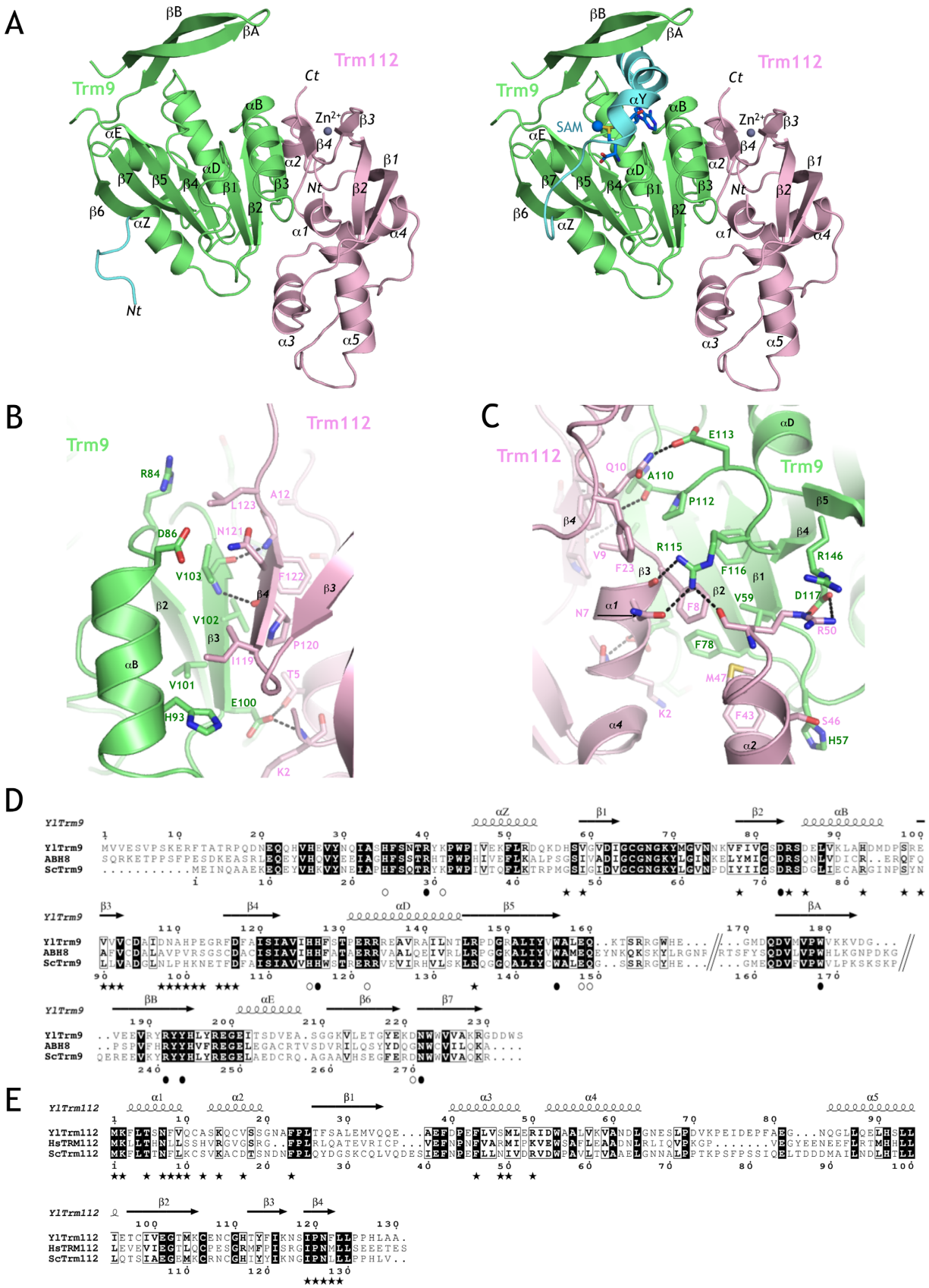

Figure 1. Structure of the *Yl*Trm9-Trm112 complex. (**A**) Ribbon representations of the crystal structure of the *Yl*Trm9N38-Trm112 complex (left) and of the model of the *Yl*Trm9N20-Trm112 complex (right). On the left panel, residues 39–44, which adopt different conformations between our crystal

The corresponding residues from *Yl*Trm9 (residues 214–234) constitute strands ß6 and ß7 and are not directly involved in Trm112 interaction. Hence, the loss of interaction with Trm112 most likely results from incorrect folding of this Trm9 truncated form.

Active site mapping

Despite extensive efforts, we could not obtain crystals of the *Yl*Trm9-Trm112 or *Yl*Trm9N38-Trm112 complexes bound to SAM or SAH. We have then modeled a SAM molecule by superimposing onto *Yl*Trm9 structure our SAM-bound structure of the *Sc*Bud23-Trm112 complex (15) (rmsd of 2 Å over 134 Cα atoms; 19% sequence identity). We have further observed that upon SAM binding, *Sc*Bud23 N-terminal region folds as an α-helix that lies onto SAM. In addition, a similar α-helix is present in the structure of RPA2492 from *Rhodopseudomonas palustris*, the protein sharing the highest structural similarity with Trm9 (Supplementary Figure S3A; rmsd of 1.9 Å over 200 Cα atoms; 17% sequence identity; PDB code: 3E23). Finally, secondary structure predictions for the N-terminal region from Trm9 proteins strongly suggest that this region has indeed a high propensity to fold as an α-helix. Based on these observations, in our model of the *Yl*Trm9-Trm112 complex bound to SAM, residues 20–45 from *Yl*Trm9 fold as two α-helices (Figure 1A) and the side chains from *Yl*Trm9 Y29 and F36 (*Sc*Trm9 Y18 and F25) match with RPA2492 Y17 and Y24, and are located onto SAM, further validating our model (Supplementary Figure S3B). Finally, in this model, the Trm9 loop connecting strands ß3 and ß4 is sandwiched between Trm112 on one side and SAM on the other. As shown for Mtq2-Trm112 (26), Trm112 could stabilize this loop and hence confer SAM binding activity to Trm9. This would then rationalize in part the role of Trm112 in Trm9 activation.

Mapping of the sequence conservation at the surface of this model reveals the presence of a patch formed by highly conserved residues centered on the SAM methyl group (Figure 2A). Several residues from this patch (H24, R29, K31, H115, H116, W145, Q149, W168, R241, Y243, D270 and N271; for clarity, *Sc*Trm9 numbering will be used in this paragraph as functional analysis were performed in *S. cerevisiae*, see Table 2 for correspondence between *S. cerevisiae* and *Y. lipolytica* numbering) or from other Trm9 regions (R122 and E148) were mutated into alanine to test their role in *S. cerevisiae* Trm9 activity. As a control, we have also considered the D72A catalytic mutant deficient in SAM binding (26). Mutations were introduced into the chromosomic copy of *S. cerevisiae TRM9* gene and the activity of these mutants was first tested *in vivo* using the zymocin killer eclipse assay. While seven mutants (H24A, K31A, H115A, R122A, E148A, Q149A and D270A) exhibited the same phenotype as WT Trm9, eight mutants (R29A, D72A, H116A, W145A, W168A, R241A, Y243A and N271A) were resistant to zymocin suggesting that their tRNA modification enzymatic activity is strongly impaired (Table 2 and Figure 2B). These eight mutants as well as two zymocin sensitive mutants (H115A and Q149A) affecting residues directly oriented toward the putative active site were selected for further functional analyses. Co-immunoprecipitation experiments demonstrated that the loss of *in vivo* activity of these mutants is not due to disruption of the Trm9-Trm112 complex (Figure 2C). This further indicated that all these mutants accumulate in the cells although to various extents depending on the mutants and that these mutations might directly impact the enzymatic activity of the complex.

All these complexes were expressed in *E. coli* and exhibited the same purification profile as the wild-type complex strongly suggesting that they are properly folded. The *S. cerevisiae* Trm9-Trm112 complex was previously demonstrated to convert cm^5U into mcm^5U using SAM as methyl donor (44) and we have confirmed this by 2D-TLC (Supplementary Figure S4A). We have further measured the *in vitro* enzymatic activity of Trm112-Trm9 mutants at pH 7.5, which corresponds to the optimum of activity (Supplementary Figure S4B and C), by using [^{3}H]-SAM and total tRNAs purified from *S. cerevisiae trm9Δ* strain as substrates. As this mixture of tRNAs contains both substrate tRNAs and non-substrate tRNAs, the latter potentially developing inhibitory effect on Trm9 activity, only apparent kinetic properties (initial velocity, specific activity, K_m and k_{cat}) could be determined. Among the mutants exhibiting zymocin resistance *in vivo*, the D72A, H116A, W145A and W168A mutants were inactive while the R29A, R241A, Y243A and N271A mutants exhibited apparent specific activities at least one order of magnitude lower than the *Sc*Trm9-Trm112 WT enzyme (Figure 2D, Table 2). The two mutants associated to the zymocin sensitivity phenotype proved to be only slightly affected (H115A) or as active (Q149A) as the wild-type enzyme, respectively. Hence, the effect of mutations on both zymocin phenotype and enzymatic activity are correlated. Interestingly, the H115A and Y243A mutants, which modify the same amount of tRNA after 1 h in our experimental conditions, exhibit sensitive and resistant zymocin phenotype, respectively. From detailed kinetics analysis, it appears that Y243A mutant ex-

structure and our model, are colored in blue. On the right panel, the modeled *Yl*Trm9 fragment encompassing residues 20–39 (helix αY) is shown in blue. The modeled SAM molecule is shown in sticks. *Yl*Trm112 secondary structure elements are labeled in italics. (**B** and **C**) Detailed views of the residues involved in *Yl*Trm9N38-Trm112 interface. Hydrogen bonds and salt bridges are show by black dotted lines. (**D**) Sequence alignments of Trm9 orthologs from *Y. lipolytica* (*Yl*Trm9), *Homo sapiens* (ABH8) and *S. cerevisiae* (*Sc*Trm9). Strictly conserved residues are in white on a black background. Partially conserved amino acids are boxed. Secondary structure elements assigned from the *Yl*Trm9N38 crystal structure are indicated above the alignment. Black stars indicate residues involved in complex formation. Filled or open circles below the alignment indicate residues, which mutation into Ala results in zymocin resistance or sensitivity, respectively. For clarity, both *Yl*Trm9 and *Sc*Trm9 numbering are indicated. Two regions corresponding to fragments present only in *Sc*Trm9 or ABH8 have been omitted. (**E**) Sequence alignments of Trm112 orthologs from *Y. lipolytica*, *Homo sapiens* and *S. cerevisiae*. Strictly conserved residues are in white on a black background. Partially conserved amino acids are boxed. Secondary structure elements assigned from the *Yl*Trm112 crystal structure are indicated above the alignment. Black stars indicate residues involved in complex formation. Panels D and E were generated using the ESPript server (49).

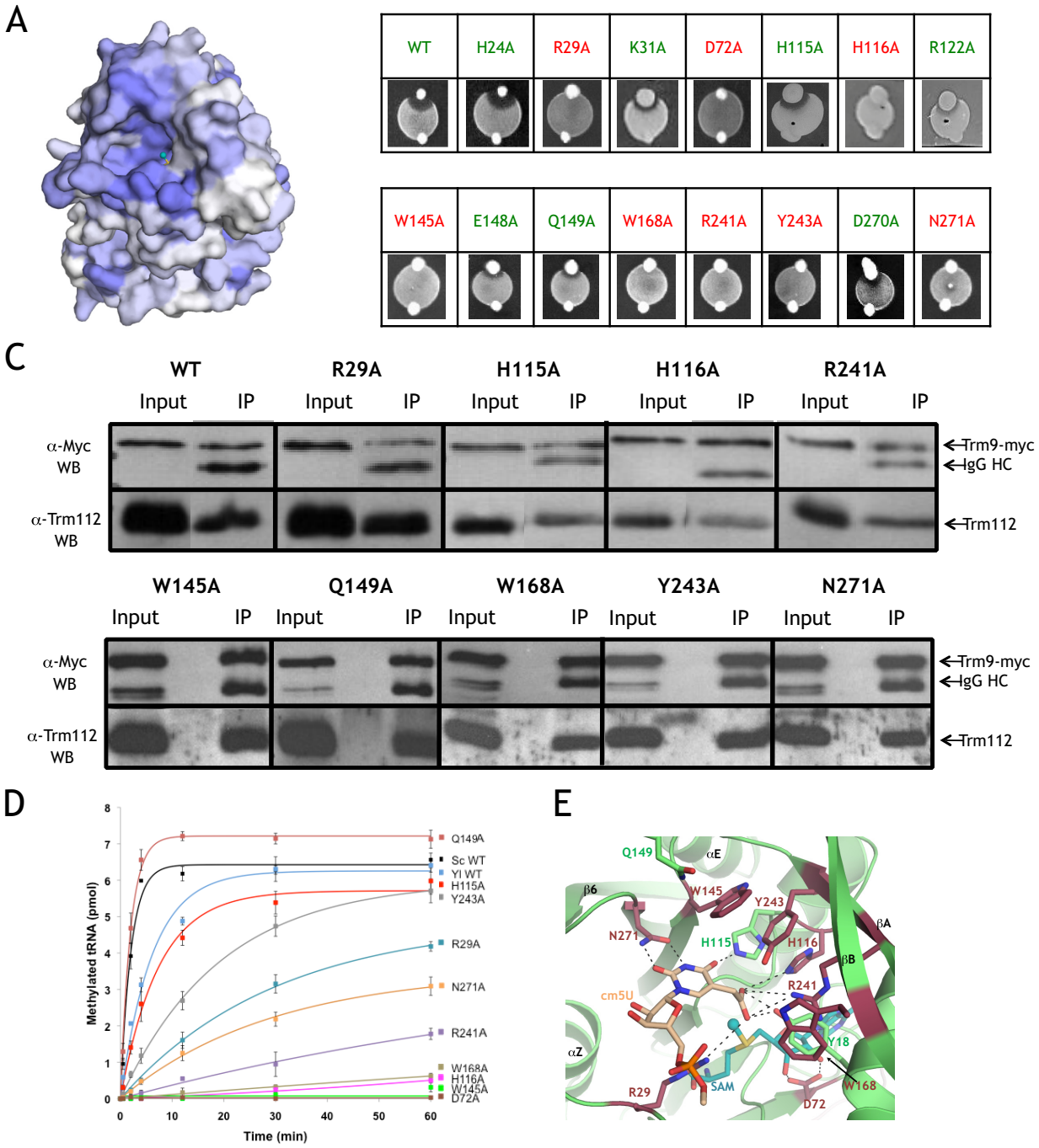

Figure 2. Trm9 active site mapping. (**A**) Mapping of the sequence conservation score at the surface of the *Yl*Trm9-Trm112 model. Coloring is from gray (low conservation) to blue (highly conserved). The conservation score was calculated using the CONSURF server (50). (**B**) Analyses of the zymocin phenotype of yeast mutant strains by eclipse assay. Each *S. cerevisiae* mutated strain was subjected to killer eclipse assay with the *Kluyveromyces lactis* AWJ137 killer strain (top) and the *Kluyveromyces lactis* NK40 non-killer strain (as a control, bottom). The presence or absence of an eclipse around the killer strain shows the sensitivity or resistance of the mutated strain to zymocin toxin, respectively. Resistant and sensitive strains are labeled in red and green, respectively. (**C**) Effect of Trm9 mutations on *Sc*Trm9/*Sc*Trm112 *in vivo* interaction. Soluble protein extracts (Input: $1/50^{th}$ of total proteins, i.e. 10 μg) and immunoprecipitates (IP: $1/10^{th}$ of immunoprecipitated material) were subjected to 15% SDS–PAGE analysis and immunoblotted using mouse anti-Myc (Trm9–13Myc) or rabbit anti-Trm112 as primary antibodies and sheep anti-mouse or sheep anti-rabbit HRP-conjugated IgG as secondary antibodies, respectively. Note that for the anti-myc probing, the lower bands observed in some of the input lanes result from Trm9-myc protein degradation whereas the band observed in the IP lanes comes from mouse primary antibody heavy chain cross-reacting with anti-mouse secondary antibody. IP were performed using 9E10 anti-myc monoclonal antibodies. (**D**) Enzymatic activity of Trm112-Trm9 mutants. The curves obtained after fitting of the experimental data with equation given in the Materials and Methods section are shown by lines using the same color code as for the symbols. (**E**) Detailed representation of the *Yl*Trm9 active site. Side chains from residues which substitution by Ala strongly (brown) or only weakly (green) affect enzymatic activity are shown as sticks. For clarity, *Sc*Trm9 numbering is used. A manually docked cm^5U nucleotide is shown as beige sticks and potential hydrogen bonds that it could form with Trm9 active site residues are depicted by dashed black lines. The modeled SAM molecule is shown as blue sticks and the methyl group to be transferred is shown as a sphere.

Table 2. Functional and enzymatic analysis of Trm9 mutants

*Sc*Trm9 mutants (*Yl*Trm9 numbering)	Zymocin sensitivity	Apparent specific activity[a]	SAM binding (%)[b]	Apparent K_m for tRNA (μM)[c]	Apparent k_{cat} for tRNA (10^{-3} s^{-1})[c]	Apparent k_{cat}/K_m for tRNA ($M^{-1}.s^{-1}$)	Apparent K_m for SAM (μM)[c]	Apparent k_{cat} for SAM (10^{-3} s^{-1})[c]	Apparent k_{cat}/K_m for SAM ($M^{-1}.s^{-1}$)
Sc WT	+	2105 ± 221	100	0.08 ± 0.02	32 ± 2	400x10^3	4.9 ± 1.1	23.7 ± 2.2	4837
H24A *(H35)*	+	ND	ND	ND	ND	ND	ND	ND	ND
R29A *(R40)*	-	108 ± 5	93 ± 21	0.936 ± 0.149	1.9 ± 0.15	2.03x10^3	5.4 ± 1.6	2.5 ±0.25	463
K31A *(K42)*	+	ND	ND	ND	ND	ND	ND	ND	ND
D72A *(D83)*	-	0	0	ND	ND	ND	ND	ND	ND
H115A *(H126)*	+	517 ± 39	143 ± 18	0.351 ± 0.118	6 ± 0.7	17.1x10^3	13.5 ± 2.8	11.7 ± 0.1	867
H116A *(H127)*	-	< 10	51 ± 5	ND	ND	ND	ND	ND	ND
R122A *(R133)*	+	ND	ND	ND	ND	ND	ND	ND	ND
W145A *(W156)*	-	< 10	85 ± 12	ND	ND	ND	ND	ND	ND
E148A *(E159)*	+	ND	ND	ND	ND	ND	ND	ND	ND
Q149A *(Q160)*	+	2498 ± 149	98 ± 18	ND	ND	ND	ND	ND	ND
W168A *(W179)*	-	< 10	46 ± 16	ND	ND	ND	ND	ND	ND
R241A *(R192)*	-	26 ± 3	173 ± 11	0.374 ± 0.008	0.8 ± 0.006	2.14x10^3	19 ± 16	0.85 ± 0.42	45
Y243A *(Y194)*	-	206 ± 5	126 ± 11	0.851 ± 0.222	4.5 ± 0.5	5.29x10^3	10 ± 3	2.9 ± 0.4	290
D270A *(D221)*	+	ND	ND	ND	ND	ND	ND	ND	ND
N271A *(N222)*	-	80 ± 3	67 ± 18	0.337 ± 0.09	1 ± 0.078	2.97x10^3	10 ± 6	0.25 ± 0.07	25
Yl WT	±	678 ± 65	ND	ND	ND	ND	ND	ND	ND

[a]Apparent specific activity (fmol of tRNA methylated/min/pmol of enzyme) calculated from apparent initial velocity. The kinetics were performed with 1.5 pmol of enzyme.
[b]These are relative values calculated fixing WT as 100%.
[c]These values were determined by fitting the data using the Michaelis–Menten equation.
ND: Not determined.

hibits reduced specific activity compared to the H115A mutant (Table 2). Therefore the threshold of Trm9 specific activity determining the cell phenotype toward zymocin lies somewhere in the window of specific activities defined by H115A and Y243A mutants. This indicates that the zymocin resistance phenotype *in vivo* is an effective tool for selecting mutants with significantly depressed Trm9 activity compared to the WT, phenotype toward zymocin switching from sensitive into resistant when *in vitro* Trm9 apparent specific activity is between 25% (H115A, sensitive) and 10% (Y243A, resistant) of the WT. We finally verified that the inactivation of these mutants did not result from defect in SAM binding using equilibrium dialysis (Table 2). As expected, the D72A mutant is inactive due to its complete loss of SAM binding capacity. The other mutants were still able to bind SAM although to different extent compared to WT complex. For these mutants, we do not observe any correlation between enzyme specific activity and SAM binding measurements, indicating that the decrease/loss of enzyme activity cannot be attributed to its reduced ability to bind SAM. Altogether, these results strongly suggest that the H116A, W145A, W168A, Y243A and to a lesser extent R29A, R241A, N271A and H115A *Sc*Trm9 mutants affect enzyme activity due to the direct involvement of these residues in catalysis or in binding of tRNA substrate.

Substrate binding and catalytic mechanism

Our site-directed mutagenesis strategy on strictly conserved residues surrounding the SAM methyl group in the *Yl*Trm9N38-Trm112 crystal structure has led to the identification of several Trm9 residues crucial for formation of mcm^5U34 in some tRNAs (Figure 2B–D). The Trm9-Trm112 complex catalyzes the O-methylation of the carboxylic function of the carboxymethyl group of cm^5U34. Due to the nucleophilic property of oxygen atoms, it is generally assumed that the methyl transfer reaction occurs through a direct SN_2 mechanism with the nucleophilic attack of the substrate (cm^5U) on the electrophilic SAM methyl group to form the methyl ester product (mcm^5U) and SAH (45). Such reaction requires the strict orientation of the incoming nucleophile to be optimal.

The comparison of previously described structures of MTases methylating carboxylic acids (i.e. TYW4 MTase, which is involved in the synthesis of wybutosine in Phe-tRNA (46), glutamate MTase CheR (47) and human LCMT-1 (48), which modifies the C-terminal leucine from PP2A) shows that two structurally conserved residues, an Arg and a Tyr (respectively R73 and Y203 in human LCMT-1), point toward the SAM methyl group and are ideally positioned to orient the substrate carboxylic group through electrostatic interactions (Supplementary Figure S5A). In our structure, the strictly conserved *Yl*Trm9 H127, corresponding to *Sc*Trm9 H116, which is crucial for enzymatic activity, structurally matches with Y203 from LCMT-1 (Supplementary Figure S5B). The H127 side chain forms a hydrogen bond with Y193 (Y242 in *Sc*Trm9) carbonyl group from strand ßB through its N∂1 atom whereas the Nϵ2 atom forms a hydrogen bond with a water molecule. This water molecule, also coordinated by H126 (*Sc*Trm9 H115), is 2.75 Å away from the SAM methyl group and is very likely to occupy the position of one of the oxygen atoms from the cm^5U carboxylic group. In our structure, no basic residue exactly matches structurally with R73 from LCMT-1. However, our mutagenesis analysis has revealed that *Sc*Trm9 R29, which is located in the Trm9 region corresponding to LCMT-1 fragment encompassing R73, is important for activity (R29 mutant enzyme exhibits only 5% of the specific activity of the WT enzyme). We then suggest that *Sc*Trm9 R29 could play the same role as R73 from LCMT-1. In *Yl*Trm9N38, R40, corresponding to *Sc*Trm9 R29, is engaged in crystal packing and is oriented in an opposite direction relative to the active site. In our model of the *Yl*Trm9 structure bound to SAM, we have oriented R40 toward the SAM methyl group. This would allow its side chain to interact with the cm^5U carboxyl group and to contribute to its correct positioning for methyl transfer (Supplementary Figure S5B). Both R40 and H127 residues in *Yl*Trm9 would then be ideally positioned to participate

in the catalysis and might play the same role as the R/Y dyad in TYW4, CheR and LCMT-1 active sites, i.e. positioning the substrate carboxylate group (cm^5U in the case of Trm9-Trm112) for the nucleophilic attack onto SAM methyl group.

Furthermore, most of the strongly affected Trm9 mutants studied here are oriented toward the SAM methyl group to be transferred onto the cm^5U and are very likely to directly participate in the optimal orientation of the cm^5U34 nucleotide from the tRNA substrates into the active site. We have then manually docked a cm^5U nucleotide into the *Yl*Trm9-Trm112 active site (Figure 2E). In this model, N222 side chain (N271 in *Sc*Trm9) forms bidentate hydrogen bonds with the O2 and N3 atoms from U34 and then could be responsible for the selective recognition of pyrimidine ring at the wobble position. H126 (H115) forms a hydrogen bond with the O4 atom from U34 allowing Trm9 discriminating between U and C. In addition, a slight reorientation of W156 side chain (W145) into the Trm9 active site would allow it to stack onto the U34 pyrimidine ring. R192 (R241) and Y29 (Y18, not mutated in this study) side chains are also within hydrogen bond distances from the cm^5U carboxylic group. Finally, the W179 indole ring (W168 in *Sc*Trm9) is solvent-exposed and could stack against the ring of a nucleotide adjacent to U34. Last but not least, in this model, the U34 3′ and 5′ positions are oriented outward the active site and hence, this model is consistent with the binding of a tRNA molecule.

We have next performed kinetic analyses on the WT, R29A, H115A, R241A, Y243A and N271A Trm9 mutants to investigate the role of these residues in tRNA modification (Table 2). Overall, compared to WT Trm9-Trm112 complex, all the mutant complexes are strongly affected in their apparent K_m for tRNA (from 4- to 12-fold increase) and in their k_{cat} (up to 100-fold decrease) whereas their K_m for SAM is much less affected (up to 4-fold). The R29A, H115A and Y243A mutants exhibit a strict correlation between the increase of K_m for tRNA and the decrease of k_{cat} which indicates these residues play an equally important role in the binding of the tRNA and in the catalysis whereas their respective K_m for SAM are either unchanged (R29A) or only slightly increased (H115A and Y243A). This clearly demonstrates the involvement of these residues in the binding of the tRNA substrate rather than in the binding of SAM. For the R241A and N271A mutants, the overall effect on K_m is the same as described above (K_m for tRNA significantly more affected than K_m for SAM) with a more dramatic decrease of k_{cat}, which may also account for the catalytic instability of these complexes during the assay. Altogether, the joint effect of mutations observed on the K_m for tRNA and k_{cat} support that the conserved residues are involved in tRNA binding and participate directly in the proper orientation of the cm^5U34 substrate into the active site, which is required for optimal methyl transfer reaction by the SN_2 mechanism.

Comparison with other Trm112-MTase complexes

Trm112 interacts with and activates four MTases that adopt (Trm9, Mtq2 and Bud23) or are predicted to adopt (Trm11) the same fold. To date, we have determined the crystal structures of complexes between Trm112 and three MTase partners (Mtq2, Bud23 and Trm9, (15, 26) and this study). Interestingly, all these 3 MTases interact in a very similar manner with Trm112 as illustrated by the superimposition of the *Yl*Trm9-Trm112 complex onto *Sc*Bud23-Trm112 (rmsd value of 2.1 Å) and *Ec*Mtq2-Trm112 complexes (rmsd value of 3 Å; Figure 3A and B). As expected from phylogenetic distance between these organisms, the Mtq2-Trm112 complex from the *E. cuniculi* parasite is the most divergent among the three complexes, and the two complexes formed by fungal proteins share more similarities. This comparison clearly indicates that the previously proposed competition between these MTases to interact with Trm112 is not due to slightly overlapping binding sites but to binding of these MTases to exactly the same region from Trm112. Although these structures are derived from complexes originating from different organisms, this offers the unique opportunity to compare their binding modes and to understand the molecular mechanisms allowing Trm112 to interact with four structurally similar MTases sharing less than 20% sequence identity within the same organism. We therefore generated a structure-based sequence alignment of *Yl*Trm9, *Ec*Mtq2 and *Sc*Bud23 and extended this alignment by including *Sc*Mtq2, *Sc*Trm9 and *Sc*Trm11 sequences (Figure 3A). From this alignment, we assume that *Sc*Mtq2 and *Sc*Trm9 residues that align with *Ec*Mtq2 and *Yl*Trm9 residues involved in the interaction with *Ec*Trm112 and *Yl*Trm112, respectively, are also contacting *Sc*Trm112. As previous studies have shown that over-expression of *Sc*Trm9 decreases the amount of *Sc*Trm11 immunoprecipitated with *Sc*Trm112 (11), we also assume that Trm11 and Trm112 interact the same way, although no structure of this complex is available yet. Hence, we propose that *Sc*Trm11 residues aligning with interface residues from the other MTases are engaged in the interaction with *Sc*Trm112 (Figure 3A).

The structural comparison between these Trm112-MTase complexes as well as the structure-based alignment of the MTase proteins allow us to identify several common features, which could explain the ability of Trm112 to interact with its four MTase partners. First, a ß-zipper interaction is formed between strand ß4 from Trm112 and strand ß3 from the various MTases (Figure 3B). Such interaction mode implies formation of a hydrogen bond network between main chain atoms from both partners and hence is less altered by side chain variations at these positions of the four MTases. Second, Trm112 shields from the solvent a hydrophobic zone on these three MTases. Although the side chains corresponding to this hydrophobic core in the four MTases from *S. cerevisiae* exhibit some degree of variation (Figure 3C), the hydrophobic character of this core is conserved thereby explaining Trm112 solubilizing effect on most of these MTases. Finally, three electrostatic hot spots are conserved between fungal *Sc*Bud23-Trm112 and *Yl*Trm9-Trm112 crystal structures. The first one involves E100 from *Yl*Trm9 (N89 from *Sc*Trm9) that forms hydrogen bonds with K2 and T5 residues from *Yl*Trm112 (Supplementary Table S1; Figure 3D). *Yl*Trm9 E100 structurally matches with D94 from *Sc*Bud23, which is also engaged in hydrogen bonds with K2 and T5 residues from *Sc*Trm112. In *Sc*Mtq2 and *Sc*Trm11, the corresponding residues are

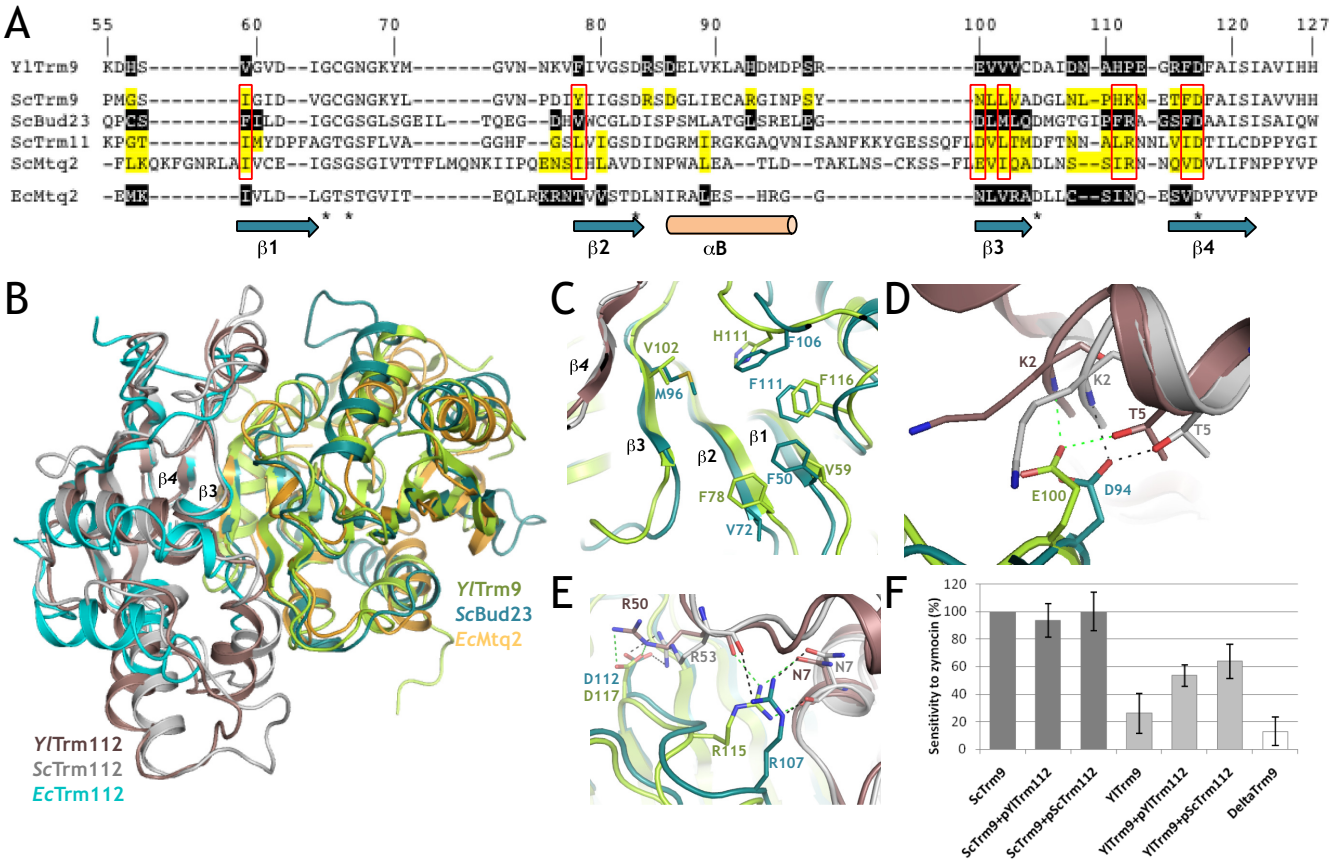

Figure 3. Structural comparison of Trm112-MTase complexes. (**A**) Structure-based sequence alignment of MTases interacting with Trm112. Only regions of these MTases that interact with Trm112 are shown. Residues directly contacting Trm112 in the X-ray structures of the complexes are in white on a black background. Residues from *Sc*Trm9, *Sc*Trm11 and *Sc*Mtq2, matching with interface residues from *Yl*Trm9 and *Ec*Mtq2, are shown in black on a yellow background. *Yl*Trm9 secondary structure elements are depicted below the alignment. Stars below the alignment indicate residues strictly conserved in all 4 *Sc*MTases considered. Residues highlighted in panels C to E are boxed in red. (**B**) Superimposition of the structures of the *Yl*Trm9-Trm112, *Sc*Bud23-Trm112 and *Ec*Mtq2-Trm112 complexes. (**C**–**E**) Detailed comparison of the hydrophobic core (C) and electrostatic hot spots (D and E) involved in *Yl*Trm9-Trm112 and *Sc*Bud23-Trm112 complexes. Same color code as panel B. (**F**) Effect of ectopic plasmid-driven expression of *Yl*Trm112 (+pYlTrm112) and *Sc*Trm112 (+pScTrm112) proteins on the susceptibility to zymocin of *S. cerevisiae* expressing either *Sc*Trm9 (dark gray) or *Yl*Trm9 (light gray) WT protein from the unique genomic copy of the corresponding gene under the control of *ScTRM9* natural promoter.

E101 and D268, respectively. Hence, in *S. cerevisiae*, the side chains found at this position of the four MTases have a similar size and possess a carbonyl group that can be engaged in hydrogen bonds with K2 and T5 from *Sc*Trm112. This is supported by our earlier observation that the substitution of N89 by Lys in *Sc*Trm9 (in combination with L91R mutation) prevents complex formation and therefore inactivates Trm9 (26). The second structurally conserved hot spot is a salt bridge formed between *Yl*Trm9 D117 with *Yl*Trm112 R50 and between *Sc*Bud23 D112 with *Sc*Trm112 R53 (Figure 3E). An Asp residue is conserved at this position in all MTases interacting with *Sc*Trm112 (Figure 3A) and we propose that a salt bridge between this Asp and *Sc*Trm112 R53 occurs in all these Trm112-Mtase complexes. We previously observed that although such interaction did not exist in the structure of the *Ec*Mtq2-Trm112 complex due to discrepancy in the Trm112 central domain containing this Arg residue, the *Sc*Trm112 R53E mutation strongly reduced the solubility and the stability of *Sc*Mtq2 and resulted in complete loss of enzyme activity (26). The third hot spot consists in three hydrogen bonds formed by *Yl*Trm9 R115 side chain with N7 main chain and side chain carbonyl groups and R50 carbonyl group from *Yl*Trm112 (Figure 3E). In our structural alignment, a basic residue is not conserved at the position corresponding to *Yl*Trm9 R115 (T104 in *Sc*Trm9, Q115 in *Sc*Mtq2, V284 in *Sc*Trm11 or S110 in *Sc*Bud23). However, the guanidinium group from *Sc*Bud23 R107 occupies exactly the same position as the guanidinium group from *Yl*Trm9 R115 and forms the same hydrogen bonding network with the N7 (also N7 in *Yl*Trm112) main chain and side chain carbonyl groups and the carbonyl group from *Sc*Trm112 R53 (R50 in *Yl*Trm9). In our alignment, the residues corresponding to *Sc*Bud23 R107 are K101 in *Sc*Trm9, R280 in *Sc*Trm11 and R112 in *Sc*Mtq2, indicating that this interaction network can exist in all these *Sc*Trm112-MTase complexes. Hence, these three crystal structures of Trm112-MTase complexes help us to understand in detail the structural plasticity that allows the small Trm112 protein to interact through the same mechanism with four MTases adopting the same fold but sharing less than 20% sequence identity.

To go deeper into the understanding of Trm112 ability to interact with various MTases, we have tested whether *Yl*Trm9, which shares 59% sequence identity with *Sc*Trm9, could functionally complement for the deletion of *TRM9* gene in *S. cerevisiae* and therefore could form a hybrid complex with *Sc*Trm112. First, we have performed enzymatic assays with the purified full-length *Yl*Trm9-Trm112 complex and tRNAs purified from *S. cerevisiae trm9Δ* strain as substrates. We observe that the *Yl* complex is functional on *S. cerevisiae* tRNAs and exhibits only a 3-fold decrease in apparent specific activity compared to *Sc* complex *in vitro* (Table 2). Furthermore, according to its apparent specific activity, the *Yl* complex should be associated with zymocin sensitivity phenotype *in vivo* (Table 2). Next, we have used an *in vivo* complementation approach in *S. cerevisiae* to characterize the biological activity of full length *Yl*Trm9. Following the replacement of genomic *ScTRM9* gene by *YlTRM9* gene (under the control of the *ScTRM9* natural promoter), the plasmid-driven expression of *Yl*Trm112 renders the strain sensitive to zymocin, indicating that an active *Yl*Trm9-*Yl*Trm112 complex can assemble and methylates *Sc* tRNAs *in vivo* (Figure 3F). In the absence of ectopic *Yl*Trm112 (i.e. in the presence of the sole endogenous *Sc*Trm112), the strain is more resistant to zymocin indicating a defect in *Yl*Trm9 activity. As *Yl*Trm9 is proved to be efficiently expressed and active in *S. cerevisiae*, the latter phenotype observed could account for the lack of interaction between *Yl*Trm9 and *Sc*Trm112. To test whether the likely competition between *Yl*Trm9 and *Sc* natural partners (Bud23, Mtq2 and Trm11) for *Sc*Trm112 could be responsible for this phenotype, we considered the potential effect of increasing *Sc*Trm112 expression level on cell phenotype toward zymocin. Plasmid-driven expression of *Sc*Trm112 resulted in zymocin sensitivity level comparable to the one previously obtained with *Yl*Trm112 (Figure 3F). This indicates that *Sc*Trm112 (50% sequence identity with *Yl*Trm112) is able to activate *Yl*Trm9 *in vivo* to a similar extent as *Yl*Trm112. This most likely occurs through a direct interaction between *Sc*Trm112 and *Yl*Trm9 (59% and 79% sequence identity and similarity with *Sc*Trm9, respectively). It should be noted that this chimeric *Yl*Trm9-*Sc*Trm112 complex is probably less stable than the corresponding complex formed by proteins from the same organism as it is necessary to increase expression level of *Sc*Trm112 to enhance zymocin sensitivity. This is further supported by preliminary co-IP experiments showing that no *Yl*Trm9-*Sc*Trm112 interaction could be characterized using a routine protocol suitable for measuring *Sc*Trm9-*Sc*Trm112 interaction.

Altogether, these results show that MTase-Trm112 binding mode is compatible with the formation of chimeric complexes between proteins from different organisms as illustrated by the ability of *Sc*Trm112 to activate *Yl*Trm9, which shares about 60% sequence identity with *Sc*Trm9. This is further supported by the ability of ABH8 (and hTrm9L) and WBSCR22 (Bud23 orthologue) human genes to partially complement the deletion of *TRM9* and *BUD23* genes in *S. cerevisiae*, respectively (24).

CONCLUSION

The structure of the Trm9-Trm112 tRNA MTase holoenzyme combined with functional studies has allowed the mapping of its active site and enabled us to propose a model of the catalytic mechanism and binding mode of the cm^5U moiety of the tRNA substrate. In addition, the detailed comparison of this structure to those of *Sc*Bud23-Trm112 and *Ec*Mtq2-Trm112 complexes highlights that during evolution, sequences of all these proteins within the same organism have evolved in a concerted manner so as to maintain the Trm112 ability to interact with its MTase partners that share less than 20% sequence identity.

ACCESSION NUMBERS

The atomic coordinates and structure factors have been deposited into the Brookhaven Protein Data Bank under accession numbers (5CM2).

SUPPLEMENTARY DATA

Supplementary Data are available at NAR Online.

ACKNOWLEDGEMENTS

We are indebted to M. Argentini and D. Cornu for mass spectrometry analysis (SICaps, IMAGIF Platform, Gif/Yvette, France), to Dr V. Heurgué-Hamard for her help with MTase assay and for sharing with us plasmids and antibodies directed against *S. cerevisiae* Trm9-Trm112 complex. We thank Dr G. Bourgeois for helpful discussion and advices. We thank Dr B. Séraphin, Dr K. Breunig and Dr R. Schaffrath for sharing reagents with us. We acknowledge SOLEIL for provision of synchrotron radiation facilities.

FUNDING

This work was supported by the Centre National pour la Recherche Scientifique (CNRS) including a specific support by the ATIP-AVENIR program [to M.G.], the European Union Sixth Framework program '3D-Repertoire' [LSHG-CT-2005-512028], the Agence Nationale pour la Recherché (ANR; ANR14-CE09-0016-02), the University Paris-Sud and Ecole Polytechnique. J.L. and T.V.N. hold a PhD fellowship from the French Ministère de l'Enseignement Supérieur et de la Recherche (MESR). Funding for open access charge: This work was supported by the Centre National pour la Recherche Scientifique (CNRS) including a specific support by the ATIP-AVENIR program [to M.G.], the European Union Sixth Framework program '3D-Repertoire' [LSHG-CT-2005-512028], the Agence Nationale pour la Recherche (ANR, ANR14-CE09-0016-02), the University Paris-Sud and Ecole Polytechnique. J.L. and T.V.N. hold a PhD fellowship from the French Ministère de l'Enseignement Supérieur et de la Recherche (MESR).
Conflict of interest statement. None declared.

REFERENCES

1. Cantara,W.A., Crain,P.F., Rozenski,J., McCloskey,J.A., Harris,K.A., Zhang,X., Vendeix,F.A., Fabris,D. and Agris,P.F. (2011) The RNA Modification Database, RNAMDB: 2011 update. *Nucleic Acids Res.*, **39**, D195–D201.

2. Hopper,A.K. and Phizicky,E.M. (2003) tRNA transfers to the limelight. *Genes Dev.*, **17**, 162–180.
3. Johansson,M.J.O. and Bystrom,A.S. (2005) In: Grosjean,H (ed). *Fine-Tuning of RNA Functions by Modification and Editing*. Springer-Verlag, Heidelberg, pp. 87–119.
4. Johansson,M.J., Esberg,A., Huang,B., Bjork,G.R. and Bystrom,A.S. (2008) Eukaryotic wobble uridine modifications promote a functionally redundant decoding system. *Mol. Cell. Biol.*, **28**, 3301–3312.
5. Huang,B., Johansson,M.J. and Bystrom,A.S. (2005) An early step in wobble uridine tRNA modification requires the Elongator complex. *RNA*, **11**, 424–436.
6. Huang,B., Lu,J. and Bystrom,A.S. (2008) A genome-wide screen identifies genes required for formation of the wobble nucleoside 5-methoxycarbonylmethyl-2-thiouridine in Saccharomyces cerevisiae. *RNA*, **14**, 2183–2194.
7. Frohloff,F., Fichtner,L., Jablonowski,D., Breunig,K.D. and Schaffrath,R. (2001) Saccharomyces cerevisiae Elongator mutations confer resistance to the Kluyveromyces lactis zymocin. *EMBO J.*, **20**, 1993–2003.
8. Glatt,S., Letoquart,J., Faux,C., Taylor,N.M., Seraphin,B. and Muller,C.W. (2012) The Elongator subcomplex Elp456 is a hexameric RecA-like ATPase. *Nat. Struct. Mol. Biol.*, **19**, 314–320.
9. Fichtner,L. and Schaffrath,R. (2002) KTI11 and KTI13, Saccharomyces cerevisiae genes controlling sensitivity to G1 arrest induced by Kluyveromyces lactis zymocin. *Mol. Microbiol.*, **44**, 865–875.
10. Kalhor,H.R. and Clarke,S. (2003) Novel methyltransferase for modified uridine residues at the wobble position of tRNA. *Mol. Cell. Biol.*, **23**, 9283–9292.
11. Studte,P., Zink,S., Jablonowski,D., Bar,C., von der Haar,T., Tuite,M.F. and Schaffrath,R. (2008) tRNA and protein methylase complexes mediate zymocin toxicity in yeast. *Mol. Microbiol.*, **69**, 1266–1277.
12. Purushothaman,S.K., Bujnicki,J.M., Grosjean,H. and Lapeyre,B. (2005) Trm11p and Trm112p are both required for the formation of 2-methylguanosine at position 10 in yeast tRNA. *Mol. Cell. Biol.*, **25**, 4359–4370.
13. Heurgue-Hamard,V., Graille,M., Scrima,N., Ulryck,N., Champ,S., van Tilbeurgh,H. and Buckingham,R.H. (2006) The zinc finger protein Ynr046w is plurifunctional and a component of the eRF1 methyltransferase in yeast. *J. Biol. Chem.*, **281**, 36140–36148.
14. White,J., Li,Z., Sardana,R., Bujnicki,J.M., Marcotte,E.M. and Johnson,A.W. (2008) Bud23 methylates G1575 of 18S rRNA and is required for efficient nuclear export of pre-40S subunits. *Mol. Cell. Biol.*, **28**, 3151–3161.
15. Letoquart,J., Huvelle,E., Wacheul,L., Bourgeois,G., Zorbas,C., Graille,M., Heurgue-Hamard,V. and Lafontaine,D.L. (2014) Structural and functional studies of Bud23-Trm112 reveal 18S rRNA N7-G1575 methylation occurs on late 40S precursor ribosomes. *Proc. Natl. Acad. Sci. U.S.A.*, **111**, E5518–E5526.
16. Sardana,R. and Johnson,A.W. (2012) The methyltransferase adaptor protein Trm112 is involved in biogenesis of both ribosomal subunits. *Mol. Biol. Cell*, **23**, 4313–4322.
17. Patil,A., Dyavaiah,M., Joseph,F., Rooney,J.P., Chan,C.T., Dedon,P.C. and Begley,T.J. (2012) Increased tRNA modification and gene-specific codon usage regulate cell cycle progression during the DNA damage response. *Cell Cycle*, **11**, 3656–3665.
18. Begley,U., Dyavaiah,M., Patil,A., Rooney,J.P., DiRenzo,D., Young,C.M., Conklin,D.S., Zitomer,R.S. and Begley,T.J. (2007) Trm9-catalyzed tRNA modifications link translation to the DNA damage response. *Mol. Cell*, **28**, 860–870.
19. Patil,A., Chan,C.T., Dyavaiah,M., Rooney,J.P., Dedon,P.C. and Begley,T.J. (2012) Translational infidelity-induced protein stress results from a deficiency in Trm9-catalyzed tRNA modifications. *RNA Biol.*, **9**, 990–1001.
20. Fu,D., Brophy,J.A., Chan,C.T., Atmore,K.A., Begley,U., Paules,R.S., Dedon,P.C., Begley,T.J. and Samson,L.D. (2010) Human AlkB homolog ABH8 Is a tRNA methyltransferase required for wobble uridine modification and DNA damage survival. *Mol. Cell. Biol.*, **30**, 2449–2459.
21. Fu,Y., Dai,Q., Zhang,W., Ren,J., Pan,T. and He,C. (2010) The AlkB domain of mammalian ABH8 catalyzes hydroxylation of 5-methoxycarbonylmethyluridine at the wobble position of tRNA. *Angew. Chem. Int. Ed. Engl.*, **49**, 8885–8888.
22. Songe-Moller,L., van den Born,E., Leihne,V., Vagbo,C.B., Kristoffersen,T., Krokan,H.E., Kirpekar,F., Falnes,P.O. and Klungland,A. (2010) Mammalian ALKBH8 possesses tRNA methyltransferase activity required for the biogenesis of multiple wobble uridine modifications implicated in translational decoding. *Mol. Cell. Biol.*, **30**, 1814–1827.
23. Shimada,K., Nakamura,M., Anai,S., De Velasco,M., Tanaka,M., Tsujikawa,K., Ouji,Y. and Konishi,N. (2009) A novel human AlkB homologue, ALKBH8, contributes to human bladder cancer progression. *Cancer Res.*, **69**, 3157–3164.
24. Begley,U., Sosa,M.S., Avivar-Valderas,A., Patil,A., Endres,L., Estrada,Y., Chan,C.T., Su,D., Dedon,P.C., Aguirre-Ghiso,J.A. *et al.* (2013) A human tRNA methyltransferase 9-like protein prevents tumour growth by regulating LIN9 and HIF1-alpha. *EMBO Mol. Med.*, **5**, 366–383.
25. Wolf,K., Breunig,K. and Barth,G. (2003) *Non-conventional yeasts in genetics, biochemistry and biotechnology : practical protocols*. Springer, Berlin; NY.
26. Liger,D., Mora,L., Lazar,N., Figaro,S., Henri,J., Scrima,N., Buckingham,R.H., van Tilbeurgh,H., Heurgue-Hamard,V. and Graille,M. (2011) Mechanism of activation of methyltransferases involved in translation by the Trm112 'hub' protein. *Nucleic Acids Res.*, **39**, 6249–6259.
27. Longtine,M.S., McKenzie,A. 3rd, Demarini,D.J., Shah,N.G., Wach,A., Brachat,A., Philippsen,P. and Pringle,J.R. (1998) Additional modules for versatile and economical PCR-based gene deletion and modification in Saccharomyces cerevisiae. *Yeast*, **14**, 953–961.
28. Toulmay,A. and Schneiter,R. (2006) A two-step method for the introduction of single or multiple defined point mutations into the genome of Saccharomyces cerevisiae. *Yeast*, **23**, 825–831.
29. Studier,F.W. (2005) Protein production by auto-induction in high density shaking cultures. *Protein Expr. Purif.*, **41**, 207–234.
30. Kabsch,W. (1993) Automatic processing of rotation diffraction data from crystals of initially unknown symmetry and cell constants. *J. Appl. Cryst.*, **26**, 795–800.
31. Adams,P.D., Grosse-Kunstleve,R.W., Hung,L.W., Ioerger,T.R., McCoy,A.J., Moriarty,N.W., Read,R.J., Sacchettini,J.C., Sauter,N.K. and Terwilliger,T.C. (2002) PHENIX: building new software for automated crystallographic structure determination. *Acta Crystallogr. D. Biol. Crystallogr.*, **58**, 1948–1954.
32. Bricogne,G., Vonrhein,C., Flensburg,C., Schiltz,M. and Paciorek,W. (2003) Generation, representation and flow of phase information in structure determination: recent developments in and around SHARP 2.0. *Acta Crystallogr. D Biol. Crystallogr.*, **59**, 2023–2030.
33. Vagin,A. and Teplyakov,A. (1997) MOLREP: an automated program for molecular replacement. *J. Appl. Cryst.*, **30**, 1022–1025.
34. Emsley,P. and Cowtan,K. (2004) Coot: model-building tools for molecular graphics. *Acta Crystallogr. D Biol. Crystallogr.*, **60**, 2126–2132.
35. Laskowski,R.A., MacArthur,M.W., Moss,D.S. and Thornton,J.M. (1993) PROCHECK: a program to check the stereochemical quality of protein structures. *J. Appl. Crystallogr.*, **26**, 283–291.
36. Chen,C., Huang,B., Anderson,J.T. and Bystrom,A.S. (2011) Unexpected accumulation of ncm(5)U and ncm(5)S(2) (U) in a trm9 mutant suggests an additional step in the synthesis of mcm(5)U and mcm(5)S(2)U. *PLoS One*, **6**, e20783.
37. Avital,S. and Elson,D. (1969) A convenient procedure for preparing transfer ribonucleic acid from Escherichia coli. *Biochim. Biophys. Acta*, **179**, 297–307.
38. Cao,W. and De La Cruz,E.M. (2013) Quantitative full time course analysis of nonlinear enzyme cycling kinetics. *Sci. Rep.*, **3**, 2658.
39. Krivov,G.G., Shapovalov,M.V. and Dunbrack,R.L. Jr (2009) Improved prediction of protein side-chain conformations with SCWRL4. *Proteins*, **77**, 778–795.
40. MacKerell,A.D., Bashford,D., Bellott, Dunbrack,R.L., Evanseck,J.D., Field,M.J., Fischer,S., Gao,J., Guo,H., Ha,S. *et al.* (1998) All-atom empirical potential for molecular modeling and dynamics studies of proteins. *J. Phys. Chem. B*, **102**, 3586–3616.
41. Brooks,B.R., Brooks,C.L. 3rd, Mackerell,A.D. Jr, Nilsson,L., Petrella,R.J., Roux,B., Won,Y., Archontis,G., Bartels,C., Boresch,S.

et al. (2009) CHARMM: the biomolecular simulation program. *J. Comput. Chem.*, **30**, 1545–1614.
42. Grosjean,H., Droogmans,L., Roovers,M. and Keith,G. (2007) Detection of enzymatic activity of transfer RNA modification enzymes using radiolabeled tRNA substrates. *Methods Enzymol.*, **425**, 55–101.
43. Sturchler,C., Lescure,A., Keith,G., Carbon,P. and Krol,A. (1994) Base modification pattern at the wobble position of Xenopus selenocysteine tRNA(Sec). *Nucleic Acids Res.*, **22**, 1354–1358.
44. Mazauric,M.H., Dirick,L., Purushothaman,S.K., Bjork,G.R. and Lapeyre,B. (2010) Trm112p is a 15-kDa zinc finger protein essential for the activity of two tRNA and one protein methyltransferases in yeast. *J. Biol. Chem.*, **285**, 18505–18515.
45. Schubert,H.L., Blumenthal,R.M. and Cheng,X. (2003) Many paths to methyltransfer: a chronicle of convergence. *Trends Biochem. Sci.*, **28**, 329–335.
46. Suzuki,Y., Noma,A., Suzuki,T., Ishitani,R. and Nureki,O. (2009) Structural basis of tRNA modification with CO2 fixation and methylation by wybutosine synthesizing enzyme TYW4. *Nucleic Acids Res.*, **37**, 2910–2925.
47. Djordjevic,S. and Stock,A.M. (1997) Crystal structure of the chemotaxis receptor methyltransferase CheR suggests a conserved structural motif for binding S-adenosylmethionine. *Structure*, **5**, 545–558.
48. Stanevich,V., Jiang,L., Satyshur,K.A., Li,Y., Jeffrey,P.D., Li,Z., Menden,P., Semmelhack,M.F. and Xing,Y. (2011) The structural basis for tight control of PP2A methylation and function by LCMT-1. *Mol. Cell*, **41**, 331–342.
49. Robert,X. and Gouet,P. (2014) Deciphering key features in protein structures with the new ENDscript server. *Nucleic Acids Res.*, **42**, W320–W324.
50. Ashkenazy,H., Erez,E., Martz,E., Pupko,T. and Ben-Tal,N. (2010) ConSurf 2010: calculating evolutionary conservation in sequence and structure of proteins and nucleic acids. *Nucleic Acids Res.*, **38**, W529–W533.